Journal of Power Sources 222 (2013) 400–409

Contents lists available at SciVerse ScienceDirect

Journal of Power Sources

journal homepage: www.elsevier.com/locate/jpowsour

Fast and reversible lithium storage in a wrinkled structure formed from Si nanoparticles during lithiation/delithiation cycling

Shinichiroh Iwamura, Hirotomo Nishihara*, Takashi Kyotani

Institute of Multidisciplinary Research for Advanced Materials, Tohoku University, 2-1-1 Katahira, Aoba-ku, Sendai 980-8577, Japan

HIGHLIGHTS

- A wrinkled structure is formed during charge/discharge cycling of Si nanoparticles.
- The wrinkled structure exhibits high capacity as well as good rate performance.
- The wrinkled structure is retained for long cycles by restricting lithiation degree.
- Uniform carbon-coating of Si nanoparticles further enhances the performance.

GRAPHICAL ABSTRACT

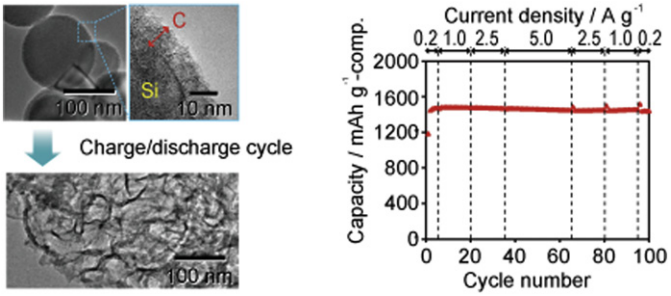

ARTICLE INFO

Article history:
Received 31 August 2012
Accepted 3 September 2012
Available online 10 September 2012

Keywords:
Silicon nanoparticles
Lithium-ion batteries
Pressure-pulsed chemical vapor deposition
Carbon-coating
Wrinkled structure

ABSTRACT

Though silicon (Si) is expected as a high capacity negative electrode for lithium-ion batteries, its drastic structure change during lithiation/delithiation cycling hampers its stable cyclability. In this work, we report that a specific structure, a wrinkled structure, is temporarily formed from Si nanoparticles (particle size was ca. 82 nm) at relatively early numbers of lithiation/delithiation cycling, and that the wrinkled structure thus formed shows a good performance. Though this structure soon transforms into a different one, resulting in fading of the performance, such transformation of the Si framework can be frozen at the state of the wrinkled structure by restricting lithiation degree. Interestingly, when Si nanoparticles are covered with a carbon nanolayer (thickness was ca. 10 nm) beforehand, the carbon layer is also deformed together with Si and is taken in by the wrinkled structure. Such carbon-coating improves the rate performance of Si nanoparticles; the carbon-coated Si nanoparticles show a constant discharge capacity of 1500 mAh g^{-1}-composite over 100 cycles and exhibit an excellent rate performance (1500 mAh g^{-1}-composite even at a rate of 3.3 C).

1. Introduction

Lithium-ion batteries (LIBs) are widely used for various mobile devices, such as cell phones, laptop computers, and recent automobiles, including fuel cell vehicles, hybrid vehicles, and electric vehicles (EVs), due to their higher energy density and lower self-discharge rate than other rechargeable batteries. [1] Their energy densities are however still not sufficient for most of the demands, especially for EVs. A typical cruising range of EVs is only less than 200 km, and it is rapidly decreased by extra energy consumption, such as lighting, air conditioning, and defrosting. The use of EV is therefore limited to short-distance driving mainly inside a big city, and the development of new-generation LIBs with further higher energy density is absolutely required. [2] Silicon (Si) attracts a great attention as a new negative electrode material for high-energy density LIBs due to its extremely higher capacity (3580 mAh g^{-1})

* Corresponding author. Tel.: +81 22 217 5627; fax: +81 22 217 5626.
E-mail address: nisihara@tagen.tohoku.ac.jp (H. Nishihara).

0378-7753/$ – see front matter © 2012 Elsevier B.V. All rights reserved.
http://dx.doi.org/10.1016/j.jpowsour.2012.09.003

than conventional graphite negative electrodes (372 mAh g^{-1}). For Si, however, there still remain several technological hurdles that should be overcome. One of the problems is a low rate performance, because of a lower electrical conductivity as well as a slower lithiation rate than graphite. This problem could be improved by making the domain size of Si down to nanometer level [3–5]. The other and much more serious problem is its poor cyclability. Upon the charging, Si is lithiated to form Si–Li alloy whose volume is 3–4 times larger than that of the original Si and then the Si–Li alloy is back to Si by the discharging. [6] Such a large volume change seriously destroys the electrode microstructure, i.e., the connections among the active materials, binder polymers, and/or conductive additives, resulting in a rapid drop of the capacity.

A lot of efforts have been made thus far to utilize Si for a negative electrode material. One method is to prepare nano-sized and/or nano-structured Si or its composite with carbon (Si/C) in which buffer space is placed around Si, so that Si can expand/recover without the destruction of a whole electrode structure. A various types of Si and Si/C composites have been synthesized, e.g., Si nanowires [7,8], Si nanotubes, [9,10] nest-like Si nanosphere [11], 3D porous Si particle [12], monodispersed Si nanoparticles [13], carbon inverse-opal decorated with Si nanolayer/nanoparticles [14,15], C/Si or Si/C core–shell nanowires [16,17], carbon nanowires/nanotubes loaded with Si nanoparticles [18], and dendritic carbon black loaded with Si nanocarticles [19]. These materials have exhibited better performances than conventional Si negative electrodes and some of them have achieved very promising performances, suggesting that the control of both the nano-/microstructures of Si remarkably improves the performance of Si. However, such Si nanomaterials are usually produced by multistep and costly processes. Thus, it is highly required to prepare Si-based negative electrodes by a simple and mass-production process. From a practical point of view, commercially available Si nanoparticles have an advantage of mass-producibility. Indeed, recent publications have indicated a great potential of Si nanoparticles: their performances are noticeably improved by optimizing electrolyte additives [20], binders [21,22], conductive additives [23], and by carbon-coating [13,24–26]. Thus, in order to realize high-performance LIBs, it is essential to develop the methods for utilizing Si nanoparticles.

Since the volume of Si is significantly changed during the charging and discharging [27], it is very important to understand the structure change of Si with the charge/discharge cycling. Long-term morphological changes have been reported so far for several types of Si nanomaterials. In the cases of the Si nanotubes [10] and Si nanowires [7,8,28–30], with repeating the charge/discharge cycling, they gradually lose their crystallinity and are becoming a kind of porous structure, but retaining the initial fibrous morphologies. As a result, their diameters are increased around 1.5 times larger than original ones upon the long cycles. In the case of the Si nanolayers formed on the carbon inverse opals, they retains their original ordered macroporous structures even after 145 cycles, despite the significant expansion of the Si nanolayers upon lithiation [14]. These works have indicated that fibrous and nano-film morphologies can be retained even after the long cycling and this must be a key for their high performance as a negative electrode. In contrast, we demonstrate in the present work that Si nanoparticles show a drastic morphological change, but still keep their performance. The charge/discharge cycling transforms the morphology of Si nanoparticles into a kind of wrinkled structure, which is completely different from the ones from the Si nanomaterials described above and from conventional Si powder (μm-sized particles). We examine the performance of the wrinkled structure, and demonstrate that this temporary structure can be frozen by restricting the degree of lithiation. In addition, the effect of carbon-coating of Si nanoparticles is discussed.

2. Experimental

2.1. Sample preparation

Si nanoparticles (#0142JS) were purchased from Nanostructured & Amorphous Materials, Inc., Houston, TX, USA. The average particle size was measured to be 82 nm, by scanning electron microscopic observation. For comparison, conventional Si powder (particle size is ca. 1 μm) was also purchased from Soekawa Chemical Co., Ltd., Tokyo, Japan. These two types of Si samples with different particle sizes are referred to as nano-Si and micro-Si, respectively.

Nano-Si was uniformly covered with a carbon nanolayer through a pressure-pulsed chemical vapour deposition (P-CVD) method [31–33] where a cycle of evacuation (60 s) followed by acetylene feed (20 vol% in N_2, for 1 s) was repeated for 300 times at 750 °C. Then, the sample was further annealed at 900 °C for 2 h under vacuum. The carbon-coated nano-Si thus obtained is referred to as nano-Si/C. The weight fraction of carbon in nano-Si/C was estimated to be 19 wt%, from the weight changes when the sample was completely burnt and/or oxidized in a thermogravimetric analyzer (TGA-51H, Shimadzu Co.) at 1400 °C for 2 h under an air flow. The detail calculation method for the carbon fraction in Si/C composites with thermogravimetry was reported in our previous work [27]. From the weight ratio of Si/carbon, the theoretical capacity of nano-Si/C was estimated to be 2970 mAh g^{-1}, assuming the theoretical capacities of Si and carbon to be 3580 [34] and 372 mAh g^{-1}, respectively.

2.2. Charge/discharge measurements and ex situ characterization of structure change

Each sample was mixed with conductive additive (Denka Black, Denki Kagaku Kogyo Kabushiki Kaisya) and binder polymers (carboxymethylcellulose (DN-10L, Daicel Fine Chem Ltd.) and styrene butadiene rubber (TRD2001, JSR Corporation)) dissolved in water. The weight ratio of these components was as follows; sample:carbon black:carboxymethylcellulose:styrene butadiene rubber = 67:11:13:9. The resulting slurry was pasted onto a copper foil. After drying at 80 °C for 1 h, the foil was cut into a circular shape (16 mm in diameter), again dried at 120 °C for 6 h under vacuum, and then packed as a working electrode in a 2032-type coin cell (Hohsen Co.) together with a lithium foil as a counter electrode, through a polypropylene separator (Celgard 2400, Celgard, LLC.). The electrolyte was 1 M $LiPF_6$ in a mixture of ethylene carbonate and diethyl carbonate (1:1 by volume). The construction of the coin cell was carried out in a glove box filled with Ar.

For obtaining Li insertion/extraction capacities, the coin cell was galvanostatically charged/discharged between 0.01 and 1.5 V versus Li/Li^+ for 100 cycles by using a battery charge/discharge unit (Hokuto Denko Co., Tokyo, Japan; HJ1001) or a potentiostat/galvanostat (BioLogic, Claix, France; VMP3). In order to obtain electrochemical impedance spectrum (EIS) during the cycling, other cells were prepared and they were charged/discharged under the same measurement conditions as above, but after the 1, 5, 20, and 100 cycles, EIS measurements were conducted at 1.5 V with an amplitude of 5 mV in the frequency range from 100 kHz to 10 mHz. Note that the results of the charge/discharge measurements in the coin cells for the EIS measurements were almost the same as those without the EIS measurements. All the electrochemical measurements were performed at 25 °C.

To investigate the structural change during the cycling, the structures of the samples before and after the charge/discharge measurements were analyzed with a transmission electron microscope (TEM; JEM-2010, JEOL Ltd.) together with selected area

electron diffraction (SAD). For this purpose, other coin cells were again constructed and were charged/discharged for 5, 20 and 100 cycles. The samples were then taken out from the coin cells, thoroughly washed with diethyl carbonate and subjected to the TEM analyses. In addition, element mapping with a resolution of several nanometers was carried out for nano-Si and nano-Si/C after 20 cycles with a scanning transmission electron microscope (STEM; Titan 80-300, FEI Co.) equipped with an energy dispersive X-ray spectroscope (EDS).

3. Results and discussion

3.1. Structure of nano-Si/C

A TEM image of nano-Si is shown in Fig. 1a. In each particle, lattice fringes corresponding to Si(111) planes are clearly observed (a clear image is shown in the Supporting Information), indicating that each Si particle is nano-sized but has a crystal structure. Such a crystal structure of Si can be confirmed also by its X-ray diffraction pattern (Supporting information). An enlarged image of nano-Si is shown as an inset of Fig. 1a, which indicates that the present nano-Si is free from a surface oxide layer [27] that could lower the performance of Si negative electrodes.

Though there have been a lot of reports on the preparation of carbon-coated Si nanoparticles [13,24–26], uniform coating of the entire surface of Si nanoparticles is always a difficult task. In this work, we used the P-CVD method that gives better coating quality than conventional coating methods including the ordinary CVD method in which a carbon source gas is continuously fed to Si [18,19]. Fig. 1b shows TEM images of nano-Si/C. We can confirm that the entire surface of the interlinked Si nanoparticles is uniformly covered with a thin carbon nanolayer with a thickness of ca. 10 nm, as shown in an inset of Fig. 1b. The carbon nanolayer doesn't have a conventional stacked structure, but the orientation of its graphene sheets is rather disordered. Indeed, a peak derived from carbon (002) is not clearly observed in an XRD pattern of nano-Si/C (Supporting information).

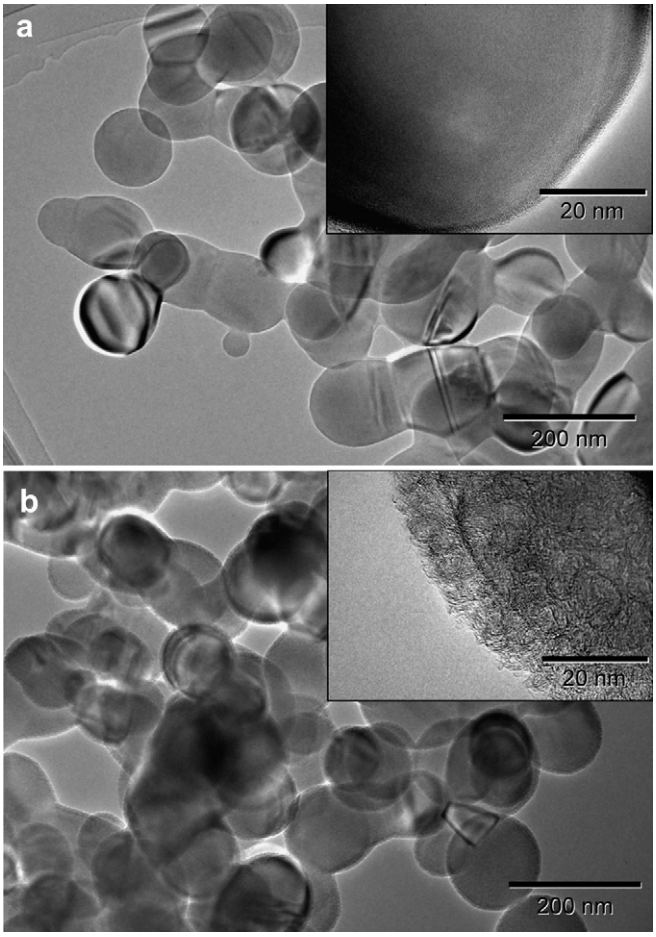

Fig. 1. TEM images of (a) nano-Si and (b) nano-Si/C. The insets represent high-magnification images.

3.2. Charge/discharge properties

Charge/discharge curves at the selected cycle numbers for micro-Si, nano-Si, and nano-Si/C are shown in Fig. 2a–c, and their corresponding differential capacity plots are shown in Fig. 2d–f. Note that all of the charge/discharge curves shown in Fig. 2 were measured at a current density of 0.2 A g^{-1}. In Fig. 2a, the 1st discharge (lithiation) capacity of micro-Si is as large as 3750 mAh g^{-1}, whereas its charge (delithiation) capacity is decreased to 2650 mAh g^{-1}. Thus, the 1st coulombic efficiency is 71%. In the following cycles, the capacity rapidly fades and the 5th charge capacity is decreased down to 430 mAh g^{-1}. Such poor cyclability is a typical behavior for bulk Si negative electrodes [35]. Its differential capacity plots (Fig. 2d) make the lithiation/delithiation process more understandable. The 1st lithiation curve shows a sharp peak at 0.1 V, corresponding to the lithiation of crystalline Si into $Li_{15}Si_4$ crystal and/or amorphous Li_xSi alloy [36,37]. On the other hand, the 1st delithiation curve shows a complex one composed of a sharp peak at 0.45 V together with a broad peak around 0.5 V, corresponding to the delithiation from crystalline $Li_{15}Si_4$ and amorphous Li_xSi alloy, respectively [36,37]. Though the 1st lithiation brings about the huge discharge capacity (3750 mAh g^{-1}), the lithium incorporated into Si is not fully released, due to the pulverization and insulation of Si. The 2nd lithiation curve shows two broad peaks around 0.25 and 0.1 V, both of which are typically seen in the lithiation of amorphous Si [37]. Though the latter peak at 0.1 V could actually include some contribution from the lithiation of crystalline Si, the drastic change from the 1st and 2nd lithiation curves clearly indicates that most of crystalline Si is transformed into amorphous upon the 1st delithiation.

The charge/discharge behavior of nano-Si (Fig. 2b and e) is noticeably different from that of micro-Si. Micro-Si shows very flat plateau both in the lithiation/delithiation curves in the 1st cycle (Fig. 2a), whereas the curves of nano-Si (Fig. 2b) has a slight slope, indicating that the formation of amorphous Li_xSi and its delithiation are dominant rather than those of $Li_{15}Si_4$ crystal. Such different behavior depending on the particle size agrees with previous literature: bulk Si is lithiated into crystalline $Li_{15}Si_4$, whereas nano-sized Si is likely to be lithiated into amorphous Li_xSi alloy [34,38,39]. As is found from Fig. 2b, nano-Si exhibits remarkably better 1st coulombic efficiency as well as better cyclability than micro-Si. The 1st discharge and charge capacities are 3630 and 3290 mAh g^{-1}, respectively, and thus the coulombic efficiency is as high as 91%. In the following cycles, the coulombic efficiency quickly approaches to 97 ~ 98%. In addition, nano-Si exhibits much better cyclability than micro-Si: the former retains a very high charge capacity of 3210 mAh g^{-1} at the 5th cycle. Thus, it is clearly found that simply by decreasing Si particle size down to several tens nanometers, the performance of Si negative electrode can be drastically improved. Nano-Si/C shows basically a charge/discharge behavior similar to that of nano-Si (Fig. 2c and f), except for its slightly lower capacity due to the presence of carbon (19 wt%). Note that the capacity of nano-Si/C shown in Fig. 2c is based on the whole mass of the composite (mAh g^{-1}-composite). The 1st

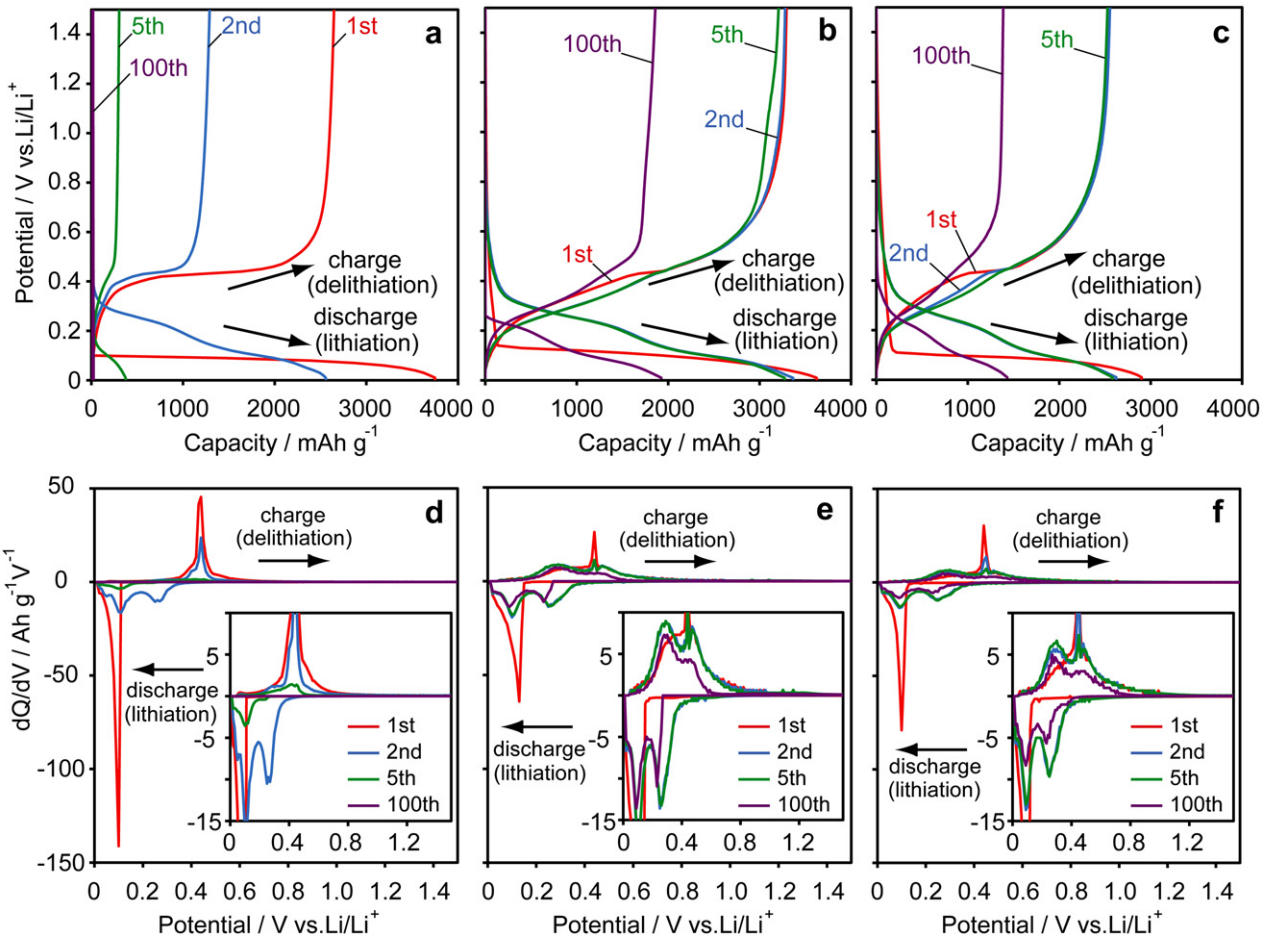

Fig. 2. Charge/discharge curves (a–c) and the corresponding differential capacity plots (d–f) of micro-Si (a, d), nano-Si (b, e) and nano-Si/C (c, f) at 1, 2, 5, and 100th cycles. In each measurement, current density was kept at 0.2 A g^{-1}. Insets are enlarged plots. The capacity of nano-Si/C is determined based on the whole mass of the composite (mAh g^{-1}-composite).

discharge and charge capacities are 2920 and 2500 mAh g^{-1}, respectively, and the coulombic efficiency is 86%. The first lithiation degree of Si in nano-Si/C corresponds to $Li_{3.7}Si$, which is almost the same as that in nano-Si ($Li_{3.5}Si$). Similar to nano-Si, nano-Si/C exhibits much better cyclability than micro-Si: its capacity at 5th cycle is as large as 2460 mAh g^{-1}.

The changes of charge/discharge capacities of each sample during 100 cycles are shown in Fig. 3a together with the changes of

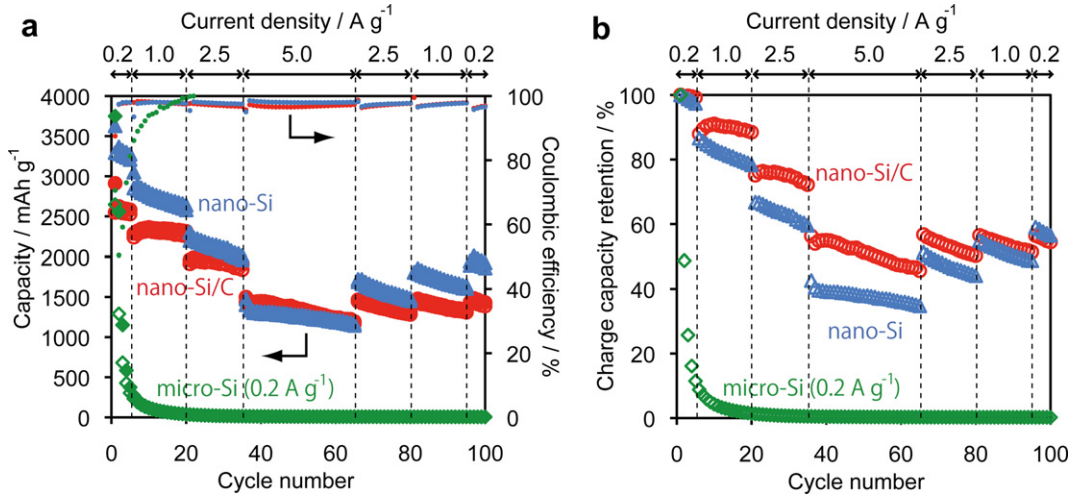

Fig. 3. (a) Charge/discharge capacities (large open/solid symbols) and coulombic efficiencies (small dots) of the samples versus cycle number. Each current density during the seven cycling periods for nano-Si and nano-Si/C is denoted above the graph, while the current density for micro-Si was constant (0.2 A g^{-1}). (b) Retention ratio of charge capacity for micro-Si, nano-Si, and nano-Si/C. Note that capacity and current density are based on the mass of the whole active materials, i.e., mAh g^{-1}-Si and A g^{-1}-Si for micro-Si and nano-Si, while mAh g^{-1}-composite and A g^{-1}-composite for nano-Si/C. Charge/discharge curves at 1, 2, 5, and 100th cycles were shown in Fig. 2a–c.

coulombic efficiency. For nano-Si and nano-Si/C, current density was altered during the cycling (see Fig. 3a for the change in current density), while a constant current density of 0.2 A g^{-1} was applied for micro-Si throughout the cycles. The charge capacity of micro-Si is rapidly decreased and almost lost at as early as 10 cycle. In marked contrast, nano-Si and nano-Si/C show much better cyclabilities than micro-Si, as were indicated also by Fig. 2. The capacity retention is plotted against the cycle number in Fig. 3b, in which nano-Si/C always shows better capacity retention at 1.0, 2.5, and 5.0 A g^{-1}, suggesting its lower inner resistance due to the presence of carbon. In both nano-Si and nano-Si/C, however, their capacities are gradually decreased with repeating charge/discharge, indicating their successive structure changes.

3.3. Structure change during lithiation/delithiation cycling

In order to understand the cyclabilities of the samples, their successive structural changes were analyzed with TEM together with SAD. Fig. 4 shows TEM images and SAD patterns of the pristine micro-Si, nano-Si, and nano-Si/C before lithiation, and their images after 5, 20, and 100 lithiation/delithiation cycles. Micro-Si before cycling (Fig. 4a) looks bulky particles with high crystallinity, which is confirmed from strong spots in its SAD pattern (inset). After 5 cycles (Fig. 4b), the structure is changed into porous-like one due to the pulverization, and the SAD pattern only shows diffuse diffraction rings, indicating that the framework becomes amorphous. From the finding that the capacity of micro-Si was almost lost at the 5th cycle (Fig. 2a), it is conjectured that most of the Si framework shown in Fig. 4b is electrically isolated because of the pulverization. Accordingly, further structure change is not apparently observed after 20 (Fig. 2c) and 100 (Fig. 2d) cycles.

On the other hand, nano-Si as well as nano-Si/C shows completely different structure changes. They are originally spherical nanoparticles with a crystalline structure (Fig. 4e and i). After 5 cycles (Fig. 4f and j), the whole frameworks are more or less aggregated, though their spherical shapes are slightly retained. The SAD patterns indicate that their structures became amorphous upon the 5 cycles. Nano-Si/C (Fig. 4j) more loses the

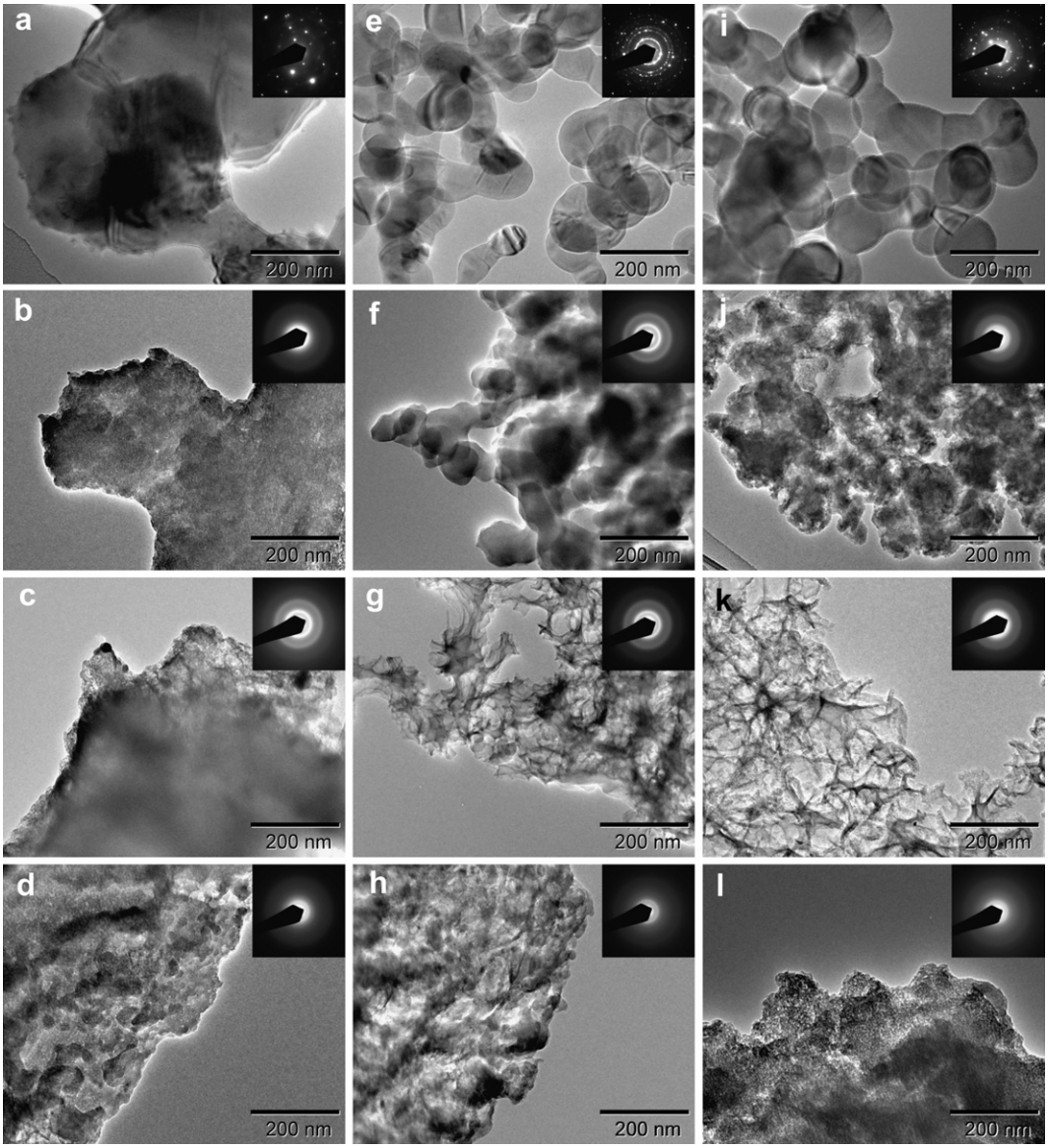

Fig. 4. TEM images and SAD patterns of (a–d) micro-Si, (e–h) nano-Si, and (i–l) nano-Si/C before and after the charge/discharge cycling: (a, e, i) the pristine samples before cycling, (b, f, j) after the 5th cycle, (c, g, k) after the 20th cycle, and (d, h, l) after the 100th cycle. The corresponding SAD patterns are shown as insets. The charge/discharge conditions are the same as that of Fig. 3.

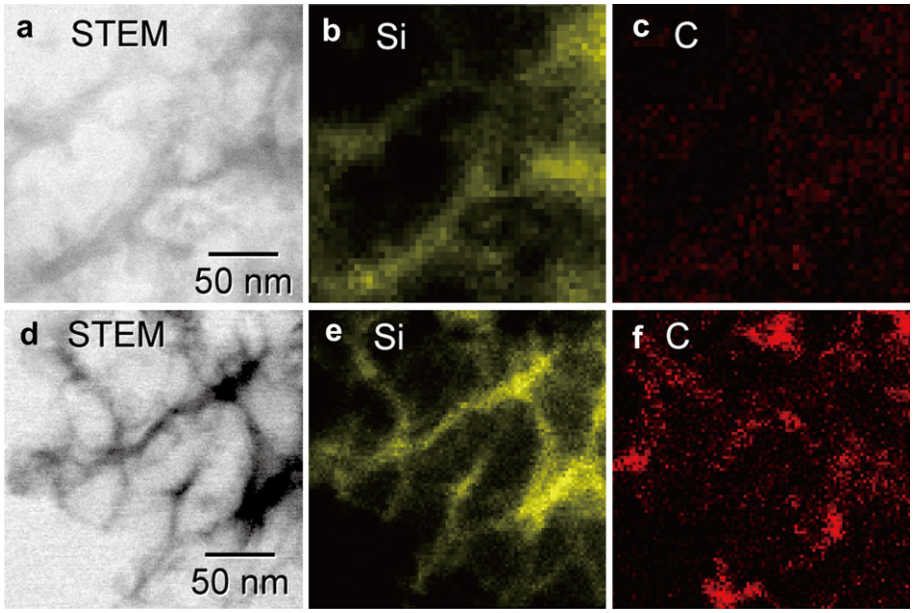

Fig. 5. STEM images and their elemental mappings of (a–c) nano-Si and (d–f) nano-Si/C after the 20th charge/discharge cycles. The elemental mappings for (b, e) Si and (c, f) C were analyzed with EDS.

original shape and more becomes a porous-like structure than nano-Si (Fig. 4f). However, the former actually exhibits better capacity retention than the latter by the 5th cycle (Fig. 3), because of the presence of carbon in the former. What is noteworthy is the drastic change in structure both for nano-Si and nano-Si/C from the 5th to 20th cycles (Fig. 4g and k). During these cycles, a kind of wrinkled structure is formed, regardless of the presence of carbon. It is noteworthy that nano-Si and nano-Si/C retain their high performance even after such drastic structure change around 20th cycle in Fig. 3. Upon the 100 cycles, however, the unique wrinkled structures are eventually transformed into a porous-like aggregation form (Fig. 4k and l), which is similar to the structure of micro-Si after 100 cycles (Fig. 4d). It is thus found that the capacity fades of nano-Si and nano-Si/C in Fig. 3 are due to their structure change from the wrinkled structure into the porous-like aggregation. Interestingly, such dynamic structure changes have never been reported for Si nanomaterials thus far, though there are a lot of publications on the structure changes of other Si nanoforms: for example, the Si nanotubes [10], Si nanowires [7,8,28–30], and carbon inverse opals [14], retain their original morphologies even after a long cycling. To our best knowledge, this is the first report for the formation of such a wrinkled structure from Si nanoparticles, although the formation mechanism is unclear up to now.

3.4. Characterization of the wrinkled structure

We then investigate the unique wrinkled structure in detail. First, EDS elemental mapping with the resolution of several nanometers was performed on the wrinkled structures formed from nano-Si and nano-Si/C after 20 charge/discharge cycles (Fig. 5). In both samples, the position of Si (Fig. 5b and e) well overlaps with the position of the wrinkles (Fig. 5a and d), indicating that the wrinkles are mainly comprised of Si. Fig. 5c shows that a small amount of C is dispersed in the wrinkled structure. The C detected in Fig. 5c is ascribed to be from binder polymers, solid–electrolyte interface, or carbon black. In nano-Si/C (Fig. 5f), the signal of C is much stronger, and more importantly, C is well dispersed and overlaps with the position of the framework (Fig. 5d). Accordingly, Fig. 5f indicates that the carbon layer in the pristine nano-Si/C is deformed together with Si during charge/discharge cycles and the carbon is dispersed in the wrinkled framework.

Next, the change in resistance components of nano-Si and nano-Si/C were analyzed with EIS. Fig. 6 shows Nyquist plots of these samples before charge/discharge measurements, and those after 1, 5, 20, and 100 cycles. In nano-Si (Fig. 6a), a semicircle at a high-frequency range is noticeably reduced after the 1st cycle, due to the amorphousization and pulverization of Si which facilitate the diffusion of Li^+ inside the Si framework [40,41]. At the 5th and the 20th cycles, the size of the semicircle is almost the same as that in the pristine sample, whereas the semicircle becomes significantly larger at the 100th cycle. These results indicate that inner resistance is greatly increased during 20–100 cycles. Probably, the wrinkled structure (formed up to the 20th cycle) retains the same level of the inner resistance as initial. In the case of nano-Si/C (Fig. 6b), the size of the semicircle remains very small even at the 20th cycle, due to the presence of carbon. However, at the 100th cycles, the semicircle eventually becomes large as the case of nano-Si. These results agree well with the tendency of the rate performances of nano-Si and nano-Si/C shown in Fig. 3. As shown in Fig. 4, the original Si-carbon core–shell structure (Fig. 4i) is drastically changed into slightly aggregated (Fig. 4j), wrinkled (Fig. 4k), and completely aggregated structures (Fig. 4l) simply by the lithiation/delithiation cycling. During such a significant structure change, carbon is also deformed together with Si. As long as the structure is the wrinkled one, nano-Si/C exhibited an adequate rate performance, due to the presence of carbon which is uniformly dispersed in the wrinkles to provide Si with a conductive path. However, further structure change into the aggregation would disconnect the carbon conductive path, thereby severely lowering its performance.

The present results suggest that nano-Si shows a good performance at least its structure change is at the state of the wrinkled structure, and that the carbon-coating of nano-Si can be effective to reduce the inner resistance. Thus, it is expected that if the structure change can be “frozen” up to the wrinkled one, the initial good performance of nano-Si could be kept over a long period.

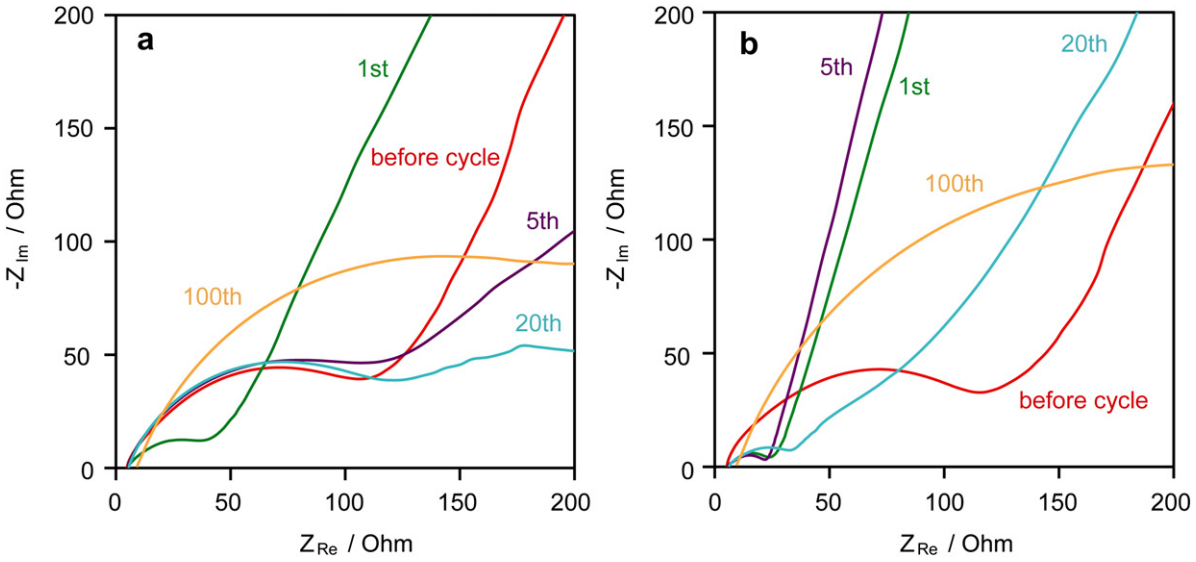

Fig. 6. Nyquist plots of (a) nano-Si and (b) nano-Si/C before the charge/discharge cycles and those after 1, 5, 20, and 100th cycles.

3.5. Freezing the structure change by the restriction of lithiation degree

Si is electrochemically lithiated during the discharge of a half cell used in this work. From the first discharge capacities of nano-Si and nano-Si/C, their lithiation degrees were estimated to be $Li_{3.5}Si$ and $Li_{3.7}Si$, respectively (Fig. 2). Based on these data, their volume expansions can be estimated. It is generally known that amorphous Li_xSi and/or a metastable crystal phase, $Li_{15}Si_4$, are formed by an electrochemical lithiation of Si at room temperature [36,37]. The $Li_{15}Si_4$ crystal corresponds to the theoretical capacity of 3572 mAh g^{-1}, and its volume is 3.8 times larger than the original Si [36]. If the density of Li_xSi alloy is proportional to the amount of Li up to 1.18 g cm^{-3} of $Li_{15}Si_4$, we can predict that nano-Si expanded up to 3.5 times its original volume. Similarly, the expansion of Si in nano-Si/C can be predicted up to 3.7 times its original volume. Such significant volume expansion may be one of the reasons for the drastic structure change of nano-Si and nano-Si/C. Since the volume expansion of Si depends on the degree of lithiation, the restriction of the lithiation degree can reduce their structure changes. It has indeed been reported that Si negative electrodes can be stably charged/discharged over a long period when the discharge (lithiation) degree is restricted [42,43]. Thus, we applied this approach to the present nano-Si and nano-Si/C. In this work, the upper limit discharge capacity was fixed to 1500 mAh g^{-1}, since further larger capacity is actually not necessary to increase an energy density of a full LIB cell, from a practical point of view. [6] Under such limitation, the lithiation degrees of Si in nano-Si and nano-Si/C are estimated to be $Li_{1.6}Si$ and $Li_{1.9}Si$, respectively, which correspond to the Si volume expansions up to 1.8 and 2.0 times their original volumes, respectively.

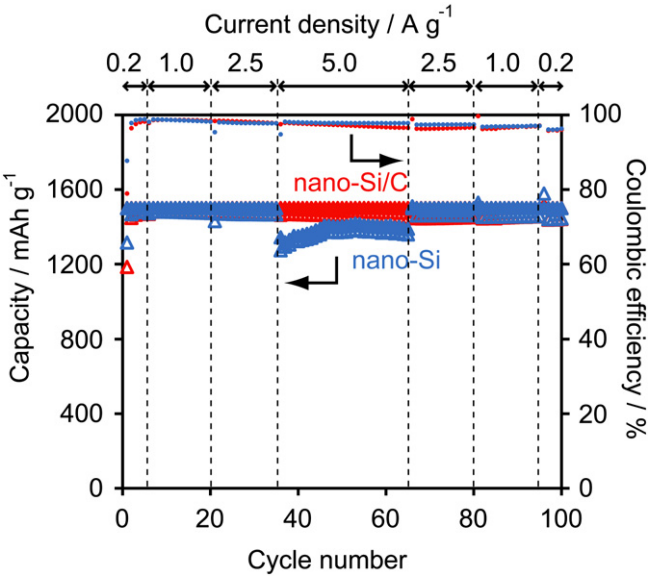

Fig. 7. Charge/discharge capacities (large open/solid symbols) and coulombic efficiencies (dots) of nano-Si and nano-Si/C versus cycle number. For both samples, discharge-capacity was restricted up to 1500 mAh g^{-1}. Cut-off potential in charging was 1.5 V vs Li/Li^+. Current density was changed from 0.2 to 5.0 A g^{-1}. The capacity of nano-Si/C is based on the whole composite mass (mAh g^{-1}-composite).

Fig. 7 shows the results of charge/discharge measurements of nano-Si and nano-Si/C with setting an upper limit of the discharge capacity to 1500 mAh g^{-1}. Note that the current density was changed between 0.2, 1.0, 2.5, and 5.0 A g^{-1}, during the charge/discharge cycling similar to the profile in Fig. 3. Since the maximum capacity is 1500 mAh g^{-1}, the corresponding C-rates are 0.13, 0.67, 1.7, and 3.3 C, respectively. Throughout the cycling, both of nano-Si and nano-Si/C exhibit very stable capacity retention except for between 36 and 65th cycle at a very high current density of 5 A g^{-1}. At this region, nano-Si shows some capacity fade, whereas nano-Si/C retains a constant discharge capacity of 1500 mAh g^{-1}. Thus, nano-Si/C can be fully discharged only within 18 min, despite its very high capacity of 1500 mAh g^{-1}, corresponding to 4 times larger capacity of the conventional graphite negative electrodes (372 mAh g^{-1}). There have been several reports on excellent rate performances of nanostructured Si negative electrodes: Si/C core/shell nanowires synthesized by the hard-template technique showed 2500 mAh g^{-1} at 6 A g^{-1} (2C) [17], and dendritic carbon black loaded with Si nanoparticles showed 1500 mAh g^{-1} at 3 A g^{-1} (1 C) [19]. Though the preparation method for Si/C composite in this work is much simpler than these high-performance materials, its performance, 1500 mAh g^{-1} at 5 A g^{-1} (3.3 C), is as good as these other materials.

Fig. 8 shows charge/discharge curves and the corresponding differential capacity plots after 1, 2, 5 and 100 cycles during the

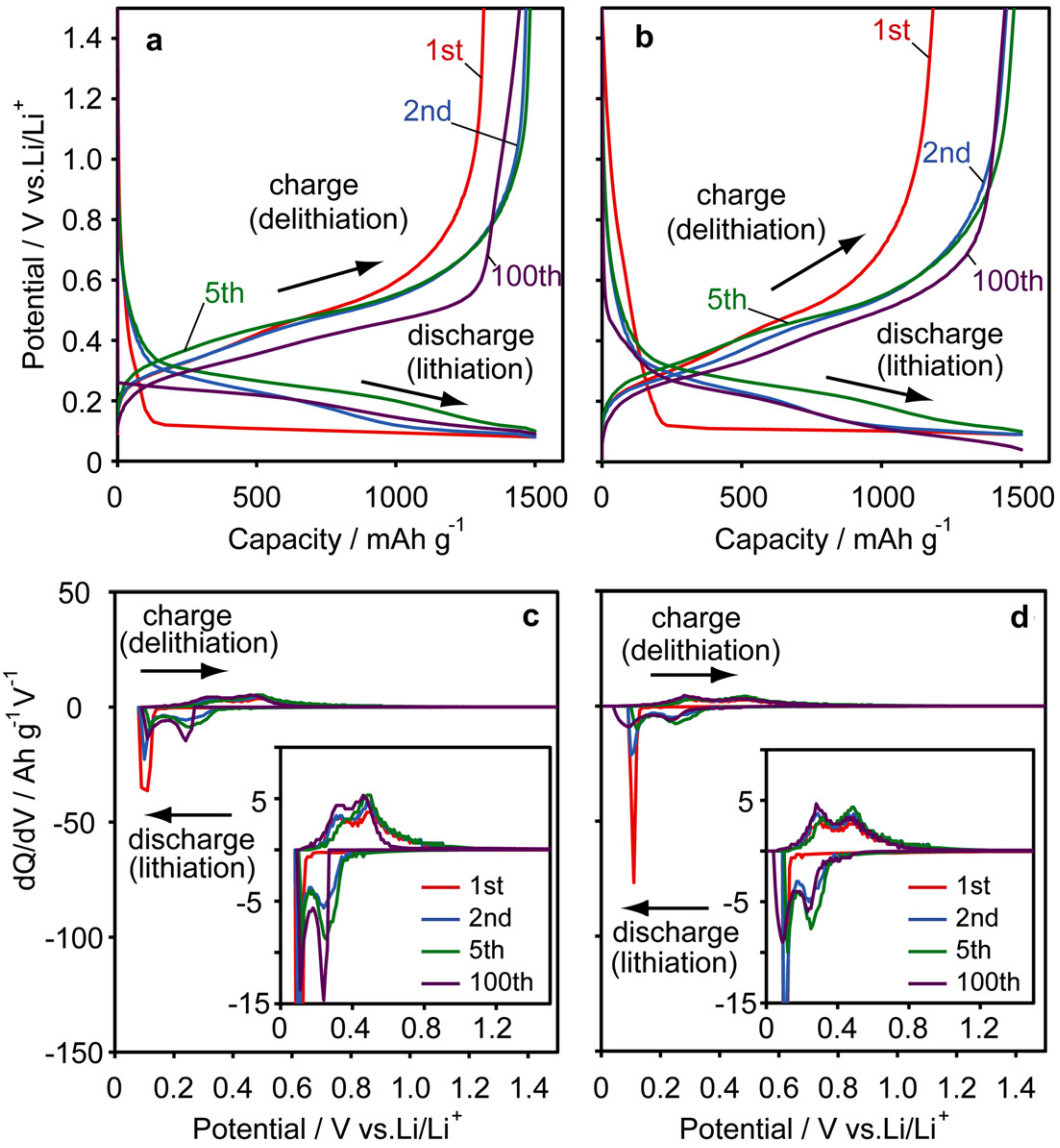

Fig. 8. Selected charge/discharge curves (a, b) and the corresponding differential capacity plots (c, d) of (a, c) nano-Si and (b, d) nano-Si/C during 100 cycles shown in Fig. 7. Insets are enlarged plots. Note that the capacity of nano-Si/C is based on the whole mass of the composite (mAh g^{-1}-composite).

measurements shown in Fig. 7. The first charge capacities of nano-Si and nano-Si/C are 1320 and 1180 mAh g^{-1} (Fig. 8a and b), and their first coulombic efficiencies are 88 and 80%, respectively. After the 2nd cycle, their charge capacities are increased to near 1500 mAh g^{-1}, and the coulombic efficiencies are quickly increased to 96 ~ 99%. In Fig. 8c and d, the charge curves of nano-Si and nano-Si/C doesn't show a sharp peak at 0.45 V, which corresponds to the delithiation from a crystalline $Li_{15}Si_4$, even in the first charge curves. Rather Fig. 8c and d display typical lithiation/delithiation patterns for amorphous Li_xSi after the first lithiation, unlike the cases of the charge/discharge without capacity limitation (Fig. 2). Accordingly, any Si in nano-Si and nano-Si/C is not deeply lithiated up to $Li_{15}Si_4$ by the capacity restriction.

Finally, the structures of nano-Si and nano-Si/C after 100 charge/discharge cycles were observed with TEM (Fig. 9). Interestingly, both structures of nano-Si (Fig. 9a) and nano-Si/C (Fig. 9b) are very similar to the structures after 20 charge/discharge cycles without capacity limitation shown in Fig. 4g and k. It is thus demonstrated that the structure change of nano-Si can be frozen at the state of the wrinkled structure by restricting the lithiation degree of Si, and under such conditions, nano-Si can be stably charged/discharged for the long period. Moreover, when nano-Si is uniformly covered with a thin carbon nanolayer beforehand, the carbon layer is deformed together with Si to form the wrinkled structure consisting of well-mixed carbon and Si. The carbon in the wrinkles still functions as a conductive path, and thus nano-Si/C exhibited better performance than nano-Si.

From a practical point of view, the use of Si nanoparticles is significantly important because they can be prepared much more easily than other types of nano-Si forms, such as nanotubes and nanowires. In addition, there are a variety of methods for the production of Si nanoparticles, such as chemical vapor deposition (CVD) [8,18,19,44–48], laser ablation [49], solution-phase reduction of Si sources such as chlorosilane [50–53], and chemical etching method [54,55]. We have proposed an easy but effective methodology to utilize Si nanoparticles in this work. Such approach would greatly contribute to further development of new-generation LIBs having high energy density as well as sufficient cyclability.

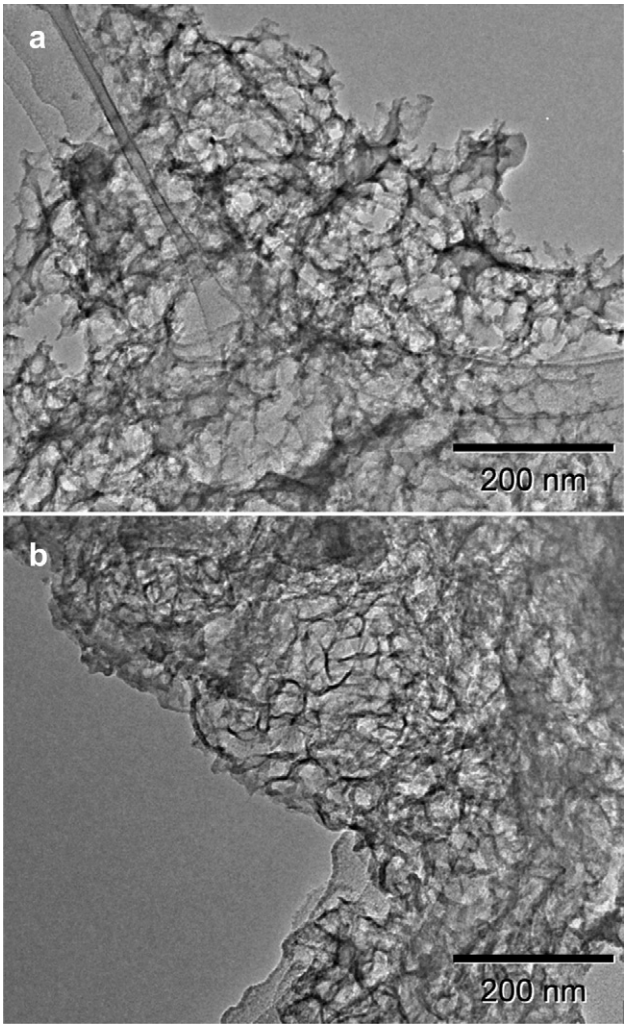

Fig. 9. TEM image of (a) nano-Si and (b) nano-Si/C after 100 charge/discharge cycles with restricting discharge capacity up to 1500 mAh g^{-1}.

4. Conclusions

The structural changes of bulk Si powder (particle size was ca. 1 μm), Si nanoparticles (particle size was ca. 82 nm) and carbon-coated Si nanoparticles during lithiation/delithiation cycling were analyzed with TEM in detail. The bulk Si was quickly transformed into a porous-like aggregated form and thus it lost 90% of its initial capacity even after the 5th cycle. On the other hand, Si nanoparticles showed a much better performance, and more importantly, their structural development is noticeably different. At 5th cycle, Si nanoparticles were slightly aggregated and fragmented, and at the 20th cycle, the structure was drastically changed into a wrinkled one, which has been discovered for the first time by the present work. Interestingly, when Si nanoparticles were covered with the carbon nanolayer beforehand, the carbon layer was also deformed together with Si and was taken in the wrinkles. The carbon in the wrinkles can play a role of conductive paths, and thus the carbon-coated sample exhibited a better rate performance than the pristine Si nanoparticles. However, the performance of the wrinkled structure gradually faded in the further cycles, and the structure was eventually changed into a completely aggregated one up to the 100th cycle. It was found that the structure development can be frozen at the state of the wrinkled structure when the lithiation degree is restricted below $Li_{1.9}Si$. In this case, the carbon-coated Si nanoparticles can enjoy a constant discharge capacity of 1500 mAh g^{-1}-composite during 100 cycles as well as an excellent rate performance (1500 mAh g^{-1}-composite even at a rate of 3.3 C). The present approach is an easy but effective method to utilize Si negative electrode and to realize high-performance LIBs with high capacity, high power, and long cycle life.

Acknowledgments

We thank Prof. Yoshimi Ohzawa (Aichi Institute of Technology) for kindly advising of the P-CVD method. We also thank Daicel Fine Chem. Ltd. and JSR Co. for kindly supplying carboxymethylcellulose and styrene butadiene rubber, respectively. This research was partially supported by a NEDO Program, Development of High-Performance Battery System for Next-Generation Vehicles (T.K.); and by the Ministry of Education, Culture, Sports, Science and Technology, Grant-in-Aid for Scientific Research on the Innovative Areas: “Fusion Materials” (Area no. 2206), 23107507 (H.N.).

Appendix A. Supplementary data

Supplementary data related to this article can be found, in the online version at, http://dx.doi.org/10.1016/j.jpowsour.2012.09.003.

References

[1] J.M. Tarascon, M. Armand, Nature 414 (2001) 359–367.
[2] H. Nishihara, T. Kyotani, Adv. Mater. 24 (2012) 4473–4498.
[3] T. Takamura, S. Ohara, M. Uehara, J. Suzuki, K. Sekine, J. Power Sources 129 (2004) 96–100.
[4] K. Yoshimura, J. Suzuki, K. Sekine, T. Takamura, J. Power Sources 146 (2005) 445–447.
[5] A. Gohier, B. Laik, J.P. Pereira-Ramos, C.S. Cojocaru, P. Tran-Van, J. Power Sources 203 (2012) 135–139.
[6] U. Kasavajjula, C.S. Wang, A.J. Appleby, J. Power Sources 163 (2007) 1003–1039.
[7] C.K. Chan, H.L. Peng, G. Liu, K. McIlwrath, X.F. Zhang, R.A. Huggins, Y. Cui, Nat. Nanotechnol 3 (2008) 31–35.
[8] L.F. Cui, R. Ruffo, C.K. Chan, H.L. Peng, Y. Cui, Nano Lett. 9 (2009) 491–495.
[9] T. Song, J.L. Xia, J.H. Lee, D.H. Lee, M.S. Kwon, J.M. Choi, J. Wu, S.K. Doo, H. Chang, W. Il Park, D.S. Zang, H. Kim, Y.G. Huang, K.C. Hwang, J.A. Rogers, U. Paik, Nano Lett. 10 (2010) 1710–1716.
[10] M.H. Park, M.G. Kim, J. Joo, K. Kim, J. Kim, S. Ahn, Y. Cui, J. Cho, Nano Lett. 9 (2009) 3844–3847.
[11] H. Ma, F.Y. Cheng, J. Chen, J.Z. Zhao, C.S. Li, Z.L. Tao, J. Liang, Adv. Mater. 19 (2007) 4067–4070.
[12] H. Kim, B. Han, J. Choo, J. Cho, Angew. Chem. Int. Ed. 47 (2008) 10151–10154.
[13] H. Kim, M. Seo, M.H. Park, J. Cho, Angew. Chem. Int. Ed. 49 (2010) 2146–2149.
[14] A. Esmanski, G.A. Ozin, Adv. Funct. Mater. 19 (2009) 1999–2010.
[15] Z.Y. Wang, F. Li, N.S. Ergang, A. Stein, Carbon 46 (2008) 1702–1710.
[16] L.F. Cui, Y. Yang, C.M. Hsu, Y. Cui, Nano Lett. 9 (2009) 3370–3374.
[17] H. Kim, J. Cho, Nano Lett. 8 (2008) 3688–3691.
[18] W. Wang, P.N. Kumta, ACS Nano 4 (2010) 2233–2241.
[19] A. Magasinski, P. Dixon, B. Hertzberg, A. Kvit, J. Ayala, G. Yushin, Nat. Mater. 9 (2010) 353–358.
[20] M.Q. Li, M.Z. Qu, X.Y. He, Z.L. Yu, Electrochim. Acta 54 (2009) 4506–4513.
[21] I. Kovalenko, B. Zdyrko, A. Magasinski, B. Hertzberg, Z. Milicev, R. Burtovyy, I. Luzinov, G. Yushin, Science 333 (2011) 75–79.
[22] A. Magasinski, B. Zdyrko, I. Kovalenko, B. Hertzberg, R. Burtovyy, C.F. Huebner, T.F. Fuller, I. Luzinov, G. Yushin, ACS Appl. Mater. Interfaces 2 (2010) 3004–3010.
[23] J. Xiao, W. Xu, D.Y. Wang, D.W. Choi, W. Wang, X.L. Li, G.L. Graff, J. Liu, J.G. Zhang, J. Electrochem. Soc. 157 (2010) A1047–A1051.
[24] S.H. Ng, J.Z. Wang, D. Wexler, K. Konstantinov, Z.P. Guo, H.K. Liu, Angew. Chem. Int. Ed. 45 (2006) 6896–6899.
[25] P.F. Gao, J.W. Fu, J. Yang, R.G. Lv, J.L. Wang, Y.N. Nuli, X.Z. Tang, Phys. Chem. Chem. Phys. 11 (2009) 11101–11105.
[26] Y.H. Xu, G.P. Yin, Y.L. Ma, P.J. Zuo, X.Q. Cheng, J. Mater. Chem. 20 (2010) 3216–3220.
[27] S. Iwamura, H. Nishihara, T. Kyotani, J. Phys. Chem. C 116 (2012) 6004–6011.
[28] J.W. Choi, J. McDonough, S. Jeong, J.S. Yoo, C.K. Chan, Y. Cui, Nano Lett. 10 (2010) 1409–1413.
[29] X.L. Chen, K. Gerasopoulos, J.C. Guo, A. Brown, C.S. Wang, R. Ghodssi, J.N. Culver, Adv. Funct. Mater. 21 (2011) 380–387.

[30] N.A. Liu, L.B. Hu, M.T. McDowell, A. Jackson, Y. Cui, ACS Nano 5 (2011) 6487–6493.
[31] Y. Ohzawa, Y. Yamanaka, K. Naga, T. Nakajima, J. Power Sources 146 (2005) 125–128.
[32] Y. Ohzawa, M. Mitani, T. Suzuki, V. Gupta, T. Nakajima, J. Power Sources 122 (2003) 153–161.
[33] H.J. Jeong, H.D. Park, J.D. Lee, J.O. Park, Carbon 34 (1996) 417–421.
[34] T.D. Hatchard, J.R. Dahn, J. Electrochem. Soc. 151 (2004) A838–A842.
[35] J.H. Ryu, J.W. Kim, Y.E. Sung, S.M. Oh, Electrochem. Solid-State Lett. 7 (2004) A306–A309.
[36] M.N. Obrovac, L. Christensen, Electrochem. Solid-State Lett. 7 (2004) A93–A96.
[37] M.N. Obrovac, L.J. Krause, J. Electrochem. Soc. 154 (2007) A103–A108.
[38] J. Saint, M. Morcrette, D. Larcher, L. Laffont, S. Beattie, J.P. Peres, D. Talaga, M. Couzi, J.M. Tarascon, Adv. Funct. Mater. 17 (2007) 1765–1774.
[39] H.S. Kim, K.Y. Chung, B.W. Cho, J. Power Sources 189 (2009) 108–113.
[40] N. Dimov, K. Fukuda, T. Umeno, S. Kugino, M. Yoshio, J. Power Sources 114 (2003) 88–95.
[41] N. Dimov, S. Kugino, M. Yoshio, Electrochim. Acta 48 (2003) 1579–1587.
[42] N. Dimov, S. Kugino, A. Yoshio, J. Power Sources 136 (2004) 108–114.
[43] W.R. Liu, J.H. Wang, H.C. Wu, D.T. Shieh, M.H. Yang, N.L. Wu, J. Electrochem. Soc. 152 (2005) A1719–A1725.
[44] W.R. Cannon, S.C. Danforth, J.H. Flint, J.S. Haggerty, R.A. Marra, J. Am. Ceram. Soc. 65 (1982) 324–330.
[45] X.G. Li, Y.Q. He, S.S. Talukdar, M.T. Swihart, Langmuir 19 (2003) 8490–8496.
[46] A. Bapat, C. Anderson, C.R. Perrey, C.B. Carter, S.A. Campbell, U. Kortshagen, Plasma Phys. Control. Fusion 46 (2004) B97–B109.
[47] R.M. Sankaran, D. Holunga, R.C. Flagan, K.P. Giapis, Nano Lett. 5 (2005) 537–541.
[48] L. Mangolini, E. Thimsen, U. Kortshagen, Nano Lett. 5 (2005) 655–659.
[49] Y. Yamada, T. Orii, I. Umezu, S. Takeyama, T. Yoshida, Jpn. J. Appl. Phys. 35 (1996) 1361–1365.
[50] J.R. Heath, Science 258 (1992) 1131–1133.
[51] R.A. Bley, S.M. Kauzlarich, J. Am. Chem. Soc. 118 (1996) 12461–12462.
[52] J.P. Wilcoxon, G.A. Samara, P.N. Provencio, Phys. Rev. B 60 (1999) 2704–2714.
[53] Q. Liu, S.M. Kauzlarich, Mater. Sci. Eng. B 96 (2002) 72–75.
[54] J.L. Heinrich, C.L. Curtis, G.M. Credo, K.L. Kavanagh, M.J. Sailor, Science 255 (1992) 66–68.
[55] R.A. Bley, S.M. Kauzlarich, J.E. Davis, H.W.H. Lee, Chem. Mater. 8 (1996) 1881–1888.